

# Inherent Proton Conduction in a 2D Coordination Framework

Daiki Umeyama,<sup>†</sup> Satoshi Horike,<sup>\*,†,‡</sup> Munehiro Inukai,<sup>§</sup> Tomoya Itakura,<sup>||</sup> and Susumu Kitagawa<sup>\*,†,§,⊥</sup>

<sup>†</sup>Department of Synthetic Chemistry and Biological Chemistry, Graduate School of Engineering, Kyoto University, Katsura, Nishikyo-ku, Kyoto 615-8510, Japan

<sup>‡</sup>PRESTO, Japan Science and Technology Agency, 4-1-8 Honcho, Kawaguchi, Saitama 332-0012, Japan

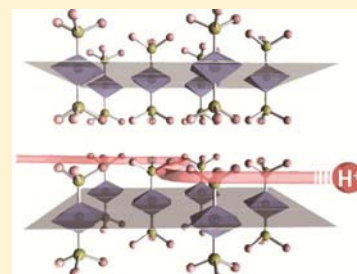
<sup>§</sup>Institute for Integrated Cell-Material Sciences (WPI-iCeMS), Kyoto University, Yoshida, Sakyo-ku, Kyoto 606-8501, Japan

<sup>||</sup>DENSO Corporation, 1-1 Showa-cho, Kariya, Aichi 448-8661, Japan

<sup>⊥</sup>ERATO, Kitagawa Integrated Pores Project, Japan Science and Technology Agency, Kyoto Research Park Building #3, Shi-mogyo-ku, Kyoto 600-8815, Japan

## Supporting Information

**ABSTRACT:** We synthesized a coordination polymer consisting of Zn<sup>2+</sup>, 1,2,4-triazole, and orthophosphates, and demonstrated for the first time intrinsic proton conduction by a coordination network. The compound has a two-dimensional layered structure with extended hydrogen bonds between the layers. It shows intrinsic proton conductivity along the direction parallel to the layers, as elucidated by impedance studies of powder and single crystals. From the low activation energy for proton hopping, the conduction mechanism was found to be of the Grotthuss fashion. The hopping is promoted by rotation of phosphate ligands, which are aligned on the layers at appropriate intervals.



## INTRODUCTION

Proton-conducting solids are one of the most important materials used in fuel cells.<sup>1</sup> Generally speaking, they are classified into two categories: intrinsic proton conductors and hybridized composite conductors. The latter is becoming the main strategy for fabricating anhydrous proton conductors at moderate temperatures (100–300 °C), which are highly needed to enhance the efficiency and reduce CO poisoning of fuel cells.<sup>2</sup> Examples of anhydrous composite conductors are polybenzimidazole (PBI)–H<sub>3</sub>PO<sub>4</sub>,<sup>3</sup> poly(ether ether ketone) (PEEK)–imidazole,<sup>4</sup> Nafion–carbon nanotubes,<sup>5</sup>  $\alpha$ -zirconium phosphate ( $\alpha$ -ZrP)–pyrazole,<sup>6</sup> CsHSO<sub>4</sub>–SiO<sub>2</sub> and CsH<sub>2</sub>PO<sub>4</sub>–SiO<sub>2</sub>,<sup>7</sup> metal–organic framework (MOF)–azoles,<sup>8</sup> and so on.<sup>9</sup> This approach could enhance the conductivity and the thermal and chemical stabilities by modulating the heterointerfaces through hybridization of proton-conductive compounds with supporting solid matrices.<sup>10</sup>

On the other hand, the development of the other class, materials with inherent proton conductivity (i.e., proton conduction by a pure-phase material itself), has great impact for primal improvement of conductivity. This class of materials is quite limited compared with the composites. CsHSO<sub>4</sub> and its family,<sup>11</sup> PBI,<sup>12</sup> and poly(vinyl phosphoric acid) (PVPA)<sup>13</sup> are a few examples. Although CsHSO<sub>4</sub> is a good proton conductor at intermediate temperature, its high water solubility, due to the fact that it is a discrete ionic crystal, is an unavoidable barrier.<sup>14</sup> Organic conductive polymers are promising candidates, but because of their amorphous nature, it is difficult to optimize the ion-hopping path and to characterize the conduction behavior. Besides these compounds, inherent proton conduction in an extended crystalline network remains challenging. This would

significantly contribute to the exploration of new proton conductors with higher performance and the elucidation of the conduction mechanism in solids as well.

The keys to attaining inherent proton conductivity include the concentration of carriers, the acidity, and the structure. Though each of them should be satisfied comprehensively, optimization of the structure is of the most importance for intrinsic conduction because it regulates the distances and dynamics of hopping sites, which dominate the mobility of protons and cooperativity of hopping. In this context, crystalline coordination networks are attractive materials because fine-tuning of the structures on the order of angstroms with a variety of functional groups is available.<sup>15</sup> Here we report the first coordination polymer with inherent anhydrous proton conductivity. We illustrate the precise design of a structure attaining the optimal network for efficient proton transport above 100 °C without any assistance of guest molecules.

## RESULTS AND DISCUSSION

We selected the phosphate group as a proton hopping site. In the coordination network, monocoordinated phosphate groups are desirable and should be located within 0.5 nm of each other to induce inherent proton hopping between them.<sup>16</sup> The coordination polymer was synthesized from zinc oxide, 1,2,4-triazole (TzH), and phosphoric acid (H<sub>3</sub>PO<sub>4</sub>) to give a white powder (hereafter **1**). The structure and chemical formula of **1** were determined by single-crystal X-ray structural analysis. As

Received: May 22, 2012

Published: July 11, 2012

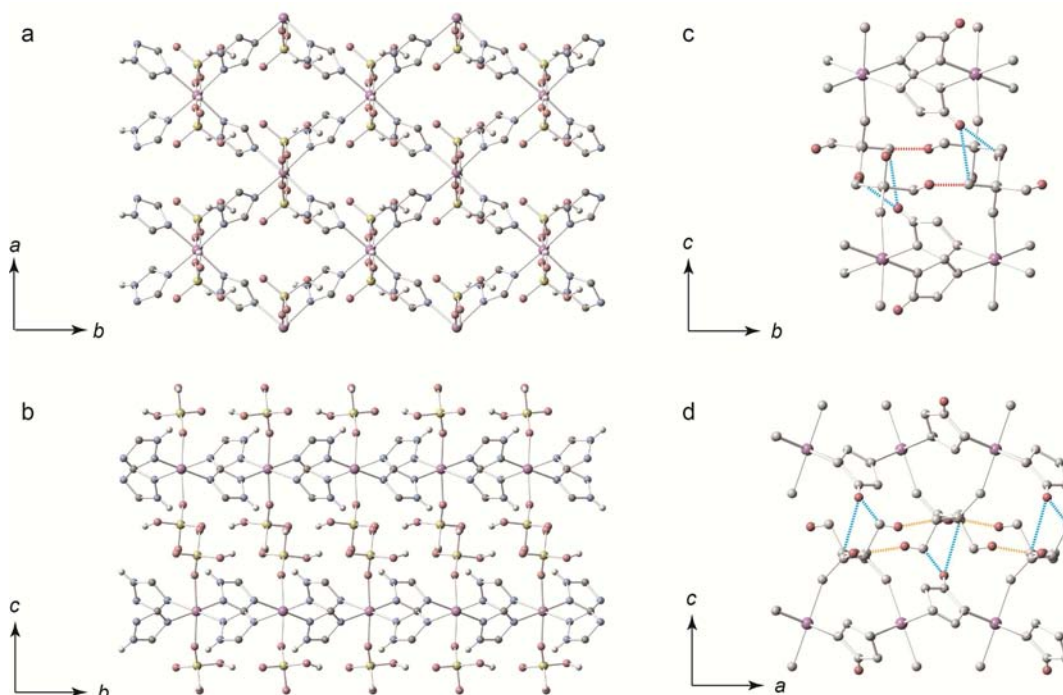


**Figure 1.** (a) Crystal structure of a 2D coordination sheet of **1**. (b) Packing structure of two 2D sheets along the *c* axis. Zn, P, O, N, C, H are purple, yellow, red, blue, gray, and white, respectively. H atoms bonded to carbons have been omitted. (c, d) Hydrogen-bonding network of **1** viewed from the (c) *a* and (d) *b* directions. Zn and H atoms are purple and red, respectively, and the other atoms are white. POH...OP (intra- and interlayer) and NH...OP (interlayer) hydrogen bonds are represented by red, orange, and blue dashed lines, respectively.

shown in Figure 1a, **1** has the formula  $[\text{Zn}(\text{H}_2\text{PO}_4)_2(\text{TzH})_2]_n$ . The coordination network is composed of octahedral  $\text{Zn}^{2+}$  with monocoordinated orthophosphate and bridging TzH, forming extended two-dimensional (2D) sheets parallel to the *ab* plane (Figure 1a). The sheets stack in the *c* direction, and the phosphates coordinate to zinc axially, forming hydrogen bonds with each other in the layers (Figure 1b–d).

In powder X-ray diffraction (PXRD), **1** showed no extra peaks derived from TzH or ZnO, and all of the peaks could be assigned to **1** (Figure S1 in the Supporting Information). Variable-temperature PXRD was also measured from ambient temperature to 180 °C (Figure S2 in the Supporting Information). The pattern remained intact from 25 to 150 °C, indicating that the original crystal structure was unchanged up to 150 °C. **1** showed an amorphous pattern at 180 °C, indicating decomposition or melting of **1**. The thermogravimetric analysis (TGA) profile of **1** shows no clear weight loss below 200 °C and a gradual decrease in mass above 200 °C (Figure 2a). The decrease is probably due to the elimination of TzH concurrent with the condensation of phosphates. Differential scanning calorimetry (DSC) showed no peak from 25 to 180 °C, and then an endothermic peak appeared at ca. 200 °C (Figure 2b). Combined with the PXRD data, the endothermic DSC peak is ascribed to the decomposition of **1** because the DSC profile did not show an exothermic peak during the cooling process.

To characterize the structure and phase purity of **1**,  $^{31}\text{P}$  cross-polarization magic-angle-spinning (CPMAS) solid-state NMR measurements were performed. Because the  $^{31}\text{P}$  chemical shift is sensitive to its coordination number and degree of condensation, the  $^{31}\text{P}$  NMR spectrum is useful to check for impurities.<sup>17</sup> The degree of condensation is represented as  $Q^n$  ( $n = 0-4$ ), where orthophosphate is  $Q^0$  and fully condensed

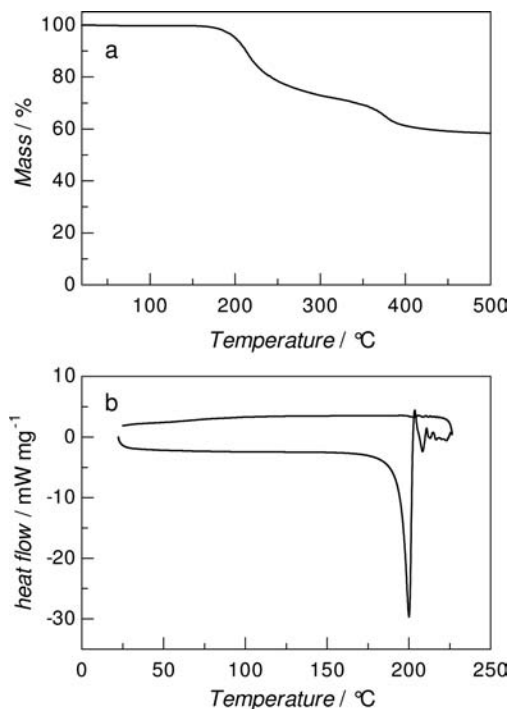


**Figure 2.** (a) TGA profile of **1** from 25 to 500 °C and (b) DSC profile of **1** from 25 to 230 °C under a  $\text{N}_2$  flow.

phosphate is  $Q^4$ . The  $^{31}\text{P}$  CPMAS NMR spectrum of **1** relative to 85%  $\text{H}_3\text{PO}_4$  is shown in Figure 3a. This spectrum denies the presence of residual  $\text{H}_3\text{PO}_4$  in **1** because there is no sharp peak at 0 ppm. In addition, diphosphoric acid and polyphosphoric acid are not formed because they show  $^{31}\text{P}$  peaks at chemical shifts beyond  $-10$  ppm. The observed peaks are regarded as

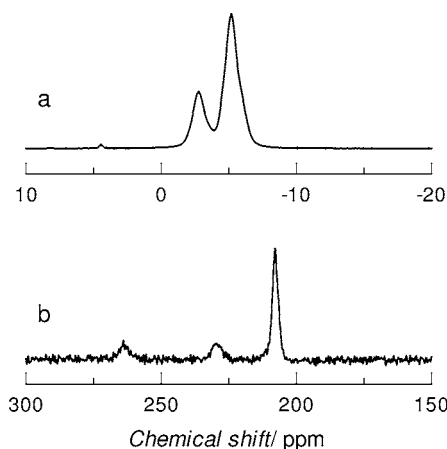


Figure 3. (a)  $^{31}\text{P}$  and (b)  $^{15}\text{N}$  CPMAS solid-state NMR spectra of **1**.

$\text{Q}^0$ , indicating the presence of monocoordinated orthophosphate.<sup>18</sup>

For intrinsic proton hopping, the positions of the protons and the fashion of the hydrogen-bonding network are important and can be determined from the crystal structure. The locations of the protons in the orthophosphate were confirmed by the bond distances between the P and O atoms, which are 1.56 Å for P–OH and 1.51 Å for P=O. Considering the charge balance, the  $\mu_2$ -triazole has to be neutral, so this framework has acidic protons not only on phosphate but also on the N(1) nitrogen atom of TzH. The position of the nitrogen atom was determined to give the best refinement in the crystal structure and to form optimal hydrogen bonds. The presence of the N–H bond in TzH was confirmed by the IR spectrum and the  $^{15}\text{N}$  CPMAS solid-state NMR spectrum. The IR spectrum shows the N–H stretch band at 2500–3500  $\text{cm}^{-1}$ , which is blue-shifted from bulk TzH, indicating that the proton is more acidic than in bulk TzH (Figure 4).<sup>19</sup> In the NMR

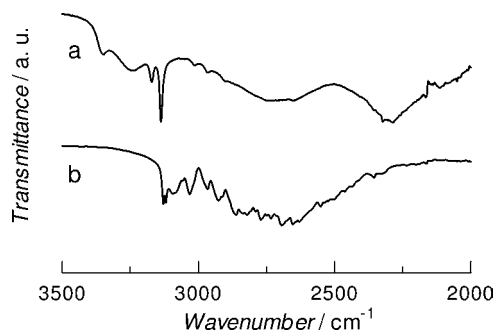


Figure 4. IR spectra of (a) **1** and (b) bulk TzH.

spectrum (Figure 3b), N(1) showed a much higher intensity than N(2) and N(4). This means that CP from H to N(1) occurs efficiently, supporting the protonation of N(1). The H on nitrogen also forms a hydrogen bond with oxygen in phosphate to make an extended hydrogen-bonding network in the *ab* plane. The hydrogen-bonding distances are 1.76 and 1.78 Å for POH...OP (2.56 and 2.57 Å for O–O) and 2.26 and 2.63 Å for NH...OP, respectively. Phosphates form intra- and interlayer hydrogen bonds, and TzH forms interlayer hydrogen bonds (Figure 1c,d). Though the structure of **1** contains acidic protons in the layer with high density, the mobile protons have to be arranged at appropriate positions for fast proton hopping

to occur in a framework. A theoretical study showed that the O–O distances of phosphates that give the minimum energy are 2.63 Å for the neutral pair ( $-\text{PO}_3\text{H}_2$  and  $-\text{PO}_3\text{H}_2$ ) and 2.52 Å for the protonated pair ( $-\text{PO}_3\text{H}_3^+$  and  $-\text{PO}_3\text{H}_2$ ).<sup>16</sup> The O–O distances in **1** were tuned to be within the ideal range described in the literature, so the formation of a protonated pair and the rearrangement of a neutral pair before and after proton hopping seem feasible. Appropriate bridging by TzH in the 2D sheet structures affords the ideal interval of 4.6–4.8 Å for phosphates, which makes all of the acidic protons hydrogen-bonded, including the proton of TzH, forming a promising structure to induce proton conduction.

The ion conductivity of **1** was measured by alternating current (AC) impedance spectroscopy from 45 to 150 °C under dry  $\text{N}_2$ . At 45 °C, although complex impedance plot looks to give single semicircle, it has two relaxation processes in the high-frequency region (Figure 5a). The complex modulus

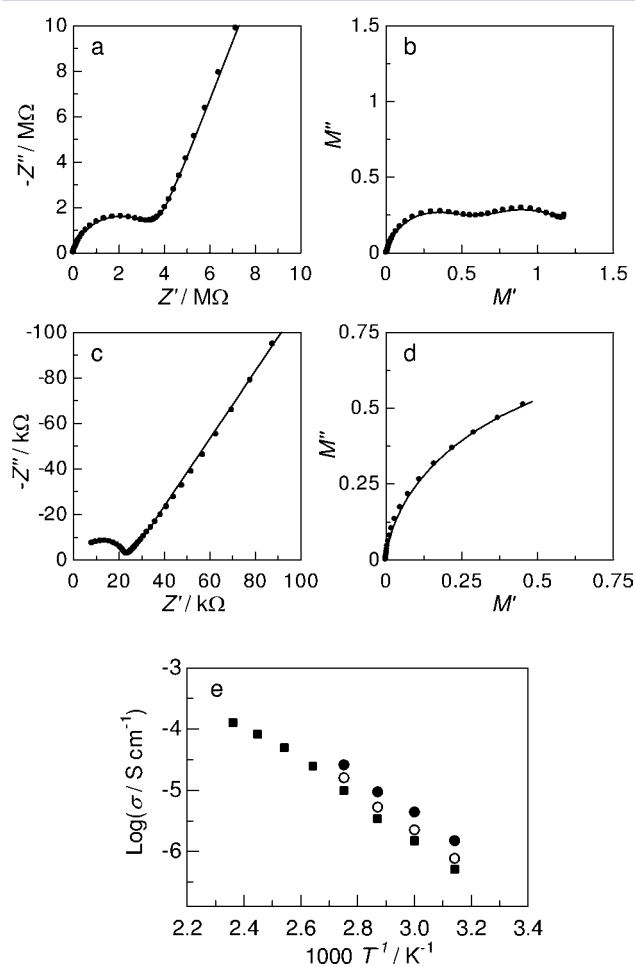


Figure 5. (a, c) Complex impedance and (b, d) modulus plots for **1** at (a, b) 45 and (c, d) 105 °C. Black ● are experimental data, and lines are simulated values from equivalent circuits. (e) Arrhenius plots of bulk (●), grain boundary (g.b.) (○), and bulk + g.b. (■) anhydrous conductivities of **1** from 45 to 150 °C.

plot (Figure 5b) makes this clear, giving two distinct semicircles; therefore, the data were fit by two series of parallel RC circuits.<sup>20</sup> Because the sample was a powder crystal, one is attributed to the bulk phase and the other to the grain boundary (g.b.).<sup>21</sup> The linear parts of the impedance plots exhibit an ion-blocking effect at the gold electrodes, which

excludes the possibility of electronic conduction. The conductivities are  $1.4 \times 10^{-6} \text{ S cm}^{-1}$  for the bulk phase and  $1.8 \times 10^{-7} \text{ S cm}^{-1}$  for the grain boundary at  $45^\circ \text{C}$ . Above  $100^\circ \text{C}$ , the two components could no longer be resolved, as shown in Figure 5c,d. This is due to a change in the resistance of **1**, causing a change in the time constants.<sup>22</sup> In this case, a single parallel RC circuit was used to fit the data, and the value is regarded as the overall conductivity (bulk + g.b.). The temperature dependences of the bulk, g.b., and overall (bulk + g.b.) conductivities ( $\sigma$ ) are plotted separately in Figure 5e, which illustrates linear increases in  $\log \sigma$ . The overall conductivity reached  $1.2 \times 10^{-4} \text{ S cm}^{-1}$  at  $150^\circ \text{C}$ , and the bulk one should be higher than this value. The Arrhenius plot for the bulk phase is linearly approximated well, and the activation energy was estimated as 0.6 eV. This value is low enough to assume that the conduction mechanism is of the Grotthuss fashion.<sup>23</sup> The result is reasonable because **1** does not contain any species that are mobile over long ranges by which protons can be transported (vehicle mechanism). Instead, they have to migrate along the architecture with hopping. These results indicate that the appropriate interval of orthophosphates in the 2D layers with the support by TzH ligands enables the intrinsic proton conduction. For instance, in  $\alpha$ -zirconium phosphate ( $\alpha$ -ZrP), another phosphate-based layered proton conductor with tricoordinated phosphate, the distance between adjacent P–OH groups is 5.3 Å, which is larger than that in **1**.<sup>24</sup> There are no hydrogen bonds between layers (only van der Waals interactions) and the interval between phosphates is too large for protons to diffuse, so  $\alpha$ -ZrP requires humidity to have enough proton conductivity.<sup>25</sup>

To obtain the direct evidence of long-range proton conduction, the direct current (DC) conductivity was confirmed by manufacturing a membrane-electrode assembly (MEA). The electromotive force of the dry  $\text{H}_2/\text{air}$  cell was measured at two different temperatures. The observed open-circuit voltage (OCV) was ca. 0.65 V at  $25^\circ \text{C}$  and 0.50 eV at  $130^\circ \text{C}$  (Figure 6). This result indicates that the conducting

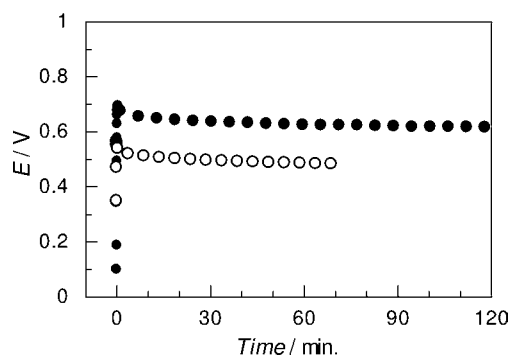


Figure 6. OCV profiles of **1** at  $25^\circ \text{C}$  (●) and  $130^\circ \text{C}$  (○).

species are protons, because oxide anions ( $\text{O}^{2-}$ ) are unlikely to be generated or move in **1** in this temperature range, and no other ions can generate an OCV in this MEA. The OCV values are lower than the theoretical maximum, which is attributed to fuel crossover, as the tendency was amplified at higher temperature.<sup>8b</sup> The fact that the OCV values were almost constant over several hours demonstrates the stability of the material under the operating conditions. The thermal stability of **1** was also checked by monitoring the conductivity while the sample was held at  $150^\circ \text{C}$ , and the conductivity did not

decrease significantly even after 7 h (Figure S3 in the Supporting Information).

To investigate in more detail the proton-conduction mechanism in the 2D sheet structure, a deuterated sample of **1** was prepared and characterized by solid-state  $^2\text{H}$  NMR spectroscopy. As  $\text{D}_3\text{PO}_4/\text{D}_2\text{O}$  was used to prepare the sample for the  $^2\text{H}$  NMR measurements, the acidic protons, including that on N(1) of TzH, were deuterated while the hydrogens bonded to carbons remained. As shown in Figure 7a, the

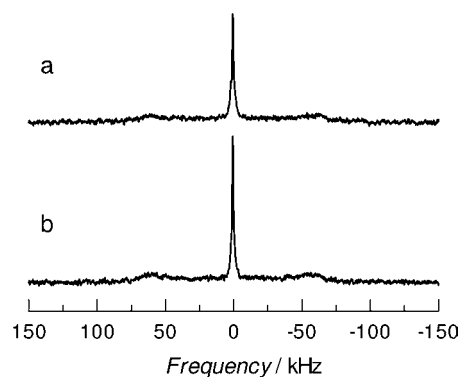
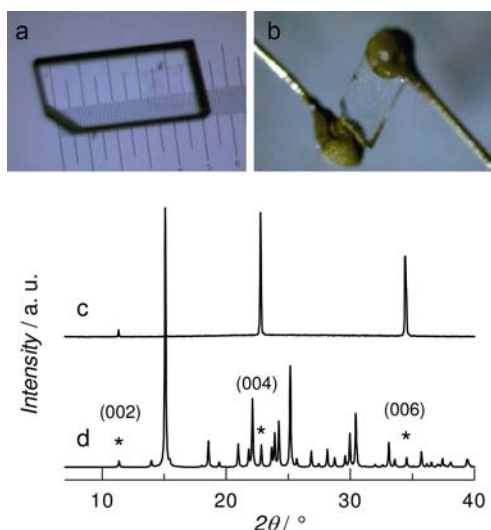


Figure 7. Solid-state  $^2\text{H}$  static NMR spectra of deuterated **1** at (a)  $25^\circ \text{C}$  and (b)  $100^\circ \text{C}$ .

spectrum of deuterated **1** at  $25^\circ \text{C}$  was isotropic, demonstrating that the interexchange of deuteriums (protons) occurs even at ambient temperature. In addition, an anisotropic peak with a spectral width of ca. 140 kHz was also observed. These observations indicate the presence of at least two components at this temperature: deuterium with high and low mobility. These two components did not disappear after the temperature was raised to  $100^\circ \text{C}$ , although the isotropic peak became sharper and more intense. This result suggests that the degree of mobility of the mobile species is increased at higher temperature, whereas the static species is still reluctant to move. One possible interpretation is that the isotropic peak represents the rotation of  $-\text{PO}_3$  group and the anisotropic peak is derived from static deuterium on the nitrogen.<sup>26</sup> This plausibly provides the idea of a proton-conduction path in the  $ab$  plane, where hydrogen-bonded phosphates are spread two-dimensionally. The conductivity of deuterated **1** was also measured, and the values decreased by ca. 2 orders of magnitude relative to **1** (Figure S4 in the Supporting Information). The difference in conductivity should be explained by quantum tunneling (or the Grotthuss mechanism) because it is sensitive to mass.

Having determined the proton conduction mechanism of **1**, we became more interested in the anisotropic ion conduction. Anisotropic ion conduction in solids is also of interest because unidirectional growth or alignment of crystals improves the performance of electrolytes.<sup>27</sup> To confirm the preferred proton-conduction path in the crystal structure, the anisotropy of the proton conductivity was evaluated by using a large single crystal of **1** (Figure 8a). The single crystal was a colorless lozenge with dimensions of  $0.55 \text{ mm} \times 0.25 \text{ mm} \times 0.06 \text{ mm}$ . To check the orientation of the crystal, the X-ray angle was scanned from  $5$  to  $40^\circ$  relative to the upper plane of the single crystal. Only three diffractions, indexed as (002), (004), and (006), were observed (Figure 8c), and thus, the upper surface was identified to be horizontal to the  $ab$  plane (perpendicular to the  $c$  axis). The out-of-plane and in-plane AC conductivities were measured by attaching gold-pasted electrodes to the crystal (Figure 8b). The



**Figure 8.** Single crystal of **1** (a) viewed from the *c* direction and (b) with gold electrolytes attached. (c) XRD pattern of the single crystal of **1** scanned from 5 to 40° relative to the *ab* plane and (d) simulated powder pattern with selected indexes.

in-plane conductivity was measured to be  $1.1 \times 10^{-4} \text{ S cm}^{-1}$  at 130 °C. This value is close to the bulk conductivity of the powder sample extrapolated from Figure 5e. Both the impedance and modulus gave a single relaxation response because of the lack of a grain boundary, and the overlap of the  $Z''$  and  $M''$  peaks in the spectra reflects long-range migration of protons (Figure 9).<sup>28</sup> The out-of-plane conductivity was  $2.9 \times$

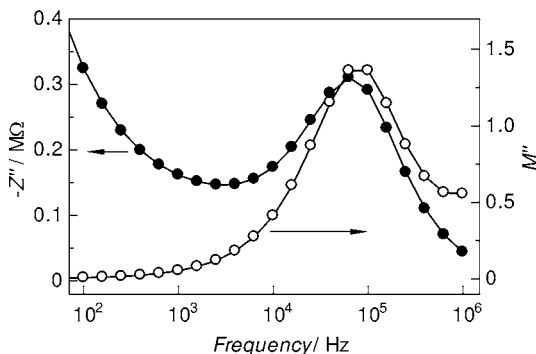


**Figure 9.** Impedance (●) and modulus (○) spectra at 130 °C for in-plane measurement.

$10^{-6} \text{ S cm}^{-1}$  at 130 °C, which is smaller than that for the in-plane direction by 2 orders of magnitude. These values are reasonable because the crystal structure indicates that protons are supposed to diffuse in the *ab* plane but not in the *c* direction. The difference between the in-plane and out-of-plane conductivities proves that the proton transport occurs in the *ab* plane, in support of the dominant conduction mechanism suggested by the  $^2\text{H}$  NMR study. The contribution of the N–H bonds of the TzH ligands as hopping sites should become effective only when the conduction is restricted to the *c* direction, while they contribute to the in-plane conductivity indirectly through the formation of hydrogen bonds.

## CONCLUSION

We have synthesized a crystalline inherent proton conductor based on an extended 2D coordination network and

characterized its anhydrous proton-conduction behavior.  $[\text{Zn}(\text{H}_2\text{PO}_4)_2(\text{TzH})_2]_n$  (**1**) consists of phosphate and triazole as the ligands, both of which retain acidic protons. These ligands are linked by extended hydrogen bonds in the layers, and **1** shows a proton conductivity of  $>10^{-4} \text{ S cm}^{-1}$  at 150 °C without any guest supports. The optimal interval for the mobile protons in the 2D layers is the key for intrinsic conduction. The anisotropic conductivity of the single crystal revealed that the proton transport occurs mainly in the *ab* plane. This result offers promising prospects for creating proton conductors by coordination-chemistry-based frameworks as well as investigating the proton-hopping mechanism in solids.<sup>29</sup>

## EXPERIMENTAL SECTION

**Synthesis of  $[\text{Zn}(\text{H}_2\text{PO}_4)_2(\text{TzH})_2]$  (**1**).** All of the chemicals and solvents used in the syntheses were reagent-grade and used without further purification. Zinc oxide (81 mg, 1 mmol), 1,2,4-triazole (138 mg, 2 mmol), and phosphoric acid (85%, 134  $\mu\text{L}$ , 2 mmol) were put into a 10 mL Teflon jar with two steel-cored 10 mm teflon balls. The mixture was ground for 60 min in a Retch MM200 grinder mill operating at 25 Hz. The powder obtained was washed with methanol and evacuated at 100 °C overnight to get dry pure-phase **1**. Deuterated **1** was obtained using  $\text{D}_3\text{PO}_4/\text{D}_2\text{O}$  (85%) instead of normal phosphoric acid.

**General Methods.** TGA was performed using a Rigaku TG8120 analyzer under flowing nitrogen with a ramp rate of 10 K  $\text{min}^{-1}$ . PXRD and variable-temperature PXRD data were collected on a Rigaku RINT 2200 Ultima diffractometer with a Cu  $K\alpha$  anode. DSC was carried out with a Mettler Toledo DSC822e/200 instrument at a heating rate of 10 K  $\text{min}^{-1}$ . IR spectra were obtained using a Nicolet ID5 attenuated total reflectance IR spectrometer operating at ambient temperature. Solid-state  $^{15}\text{N}$  and  $^{31}\text{P}$  CPMAS and  $^2\text{H}$  static NMR spectra were recorded on a Bruker Avance 400 MHz spectrometer. The spinning rate for CPMAS spectra was 8 kHz for  $^{15}\text{N}$  and 10 kHz for  $^{31}\text{P}$ .  $^2\text{H}$  spectra were recorded using a quadrupole echo pulse sequence. Single-crystal X-ray diffraction measurements were performed at 223 K with a Rigaku AFC10 diffractometer with Rigaku Saturn Kappa CCD system equipped with a MicroMax-007 HF/VariMax rotating-anode X-ray generator with confocal monochromatized Mo  $K\alpha$  radiation. Data were processed by a direct method (SIR97) and refined by full-matrix least-squares refinement using the SHELXL-97 computer program. The hydrogen atoms were positioned geometrically and refined using a riding model.

**Evaluation of Conductivity.** Impedance analysis was performed on powders of **1** without modification. The powders (ca. 50 mg) were pressed at 1000 kg N for 2 min by a standard 5 mm die and sandwiched between two gold electrodes. The impedance cell was filled with dry  $\text{N}_2$  at atmospheric pressure, and measurements were done at thermal equilibrium by holding for 30 min at each measuring temperature. The measurements were performed using an impedance and gain-phase analyzer (Solartron SI 1260) over the frequency range 1 Hz–1 MHz with an input voltage amplitude of 30 mV. ZView software was used to fit impedance data sets by means of an equivalent circuit simulation to obtain the resistance values. For OCV measurements, the MEA was prepared by the following procedure: A powder of **1** (250 mg) was sandwiched between two platinum-loaded carbon electrodes (CHEMIX, Pt loading, 2  $\text{mg cm}^{-2}$ ) in a 10 mm die and pressed at 2000 kg N for 20 min. Platinum wires were then attached to both of the electrodes. The MEA was set in a hole punched at a PTFE sheet as a gasket. Two gas chambers were set up by placing the PTFE sheet between stainless steel flanges. Dry  $\text{H}_2$  gas (100  $\text{mL min}^{-1}$ ) and dry air (100  $\text{mL min}^{-1}$ ) were supplied to the two chambers. OCV measurements were performed at 25 °C, and the voltages were monitored and collected using a data logger (KEYENCE NR-1000).

**■ ASSOCIATED CONTENT****■ Supporting Information**

PXRD patterns, time-dependent conductivity measurements, and Arrhenius plots of anhydrous conductivity. This material is available free of charge via the Internet at <http://pubs.acs.org>.

**■ AUTHOR INFORMATION****Corresponding Author**

horike@sbchem.kyoto-u.ac.jp; kitagawa@icems.kyoto-u.ac.jp

**Notes**

The authors declare no competing financial interest.

**■ ACKNOWLEDGMENTS**

This work was supported by the PRESTO Program of the Japan Science and Technology Agency, Grants-in-Aid for Scientific Research from the Japan Society for the Promotion of Science (JSPS), and the ERATO Program of the Japan Science and Technology Agency. iCeMS is supported by the World Premier International Research Initiative (WPI) of MEXT, Japan.

**■ REFERENCES**

- (1) Kreuer, K. D.; Paddison, S. J.; Spohr, E.; Schuster, M. *Chem. Rev.* **2004**, *104*, 4637.
- (2) (a) Steele, B. C. H.; Heinzel, A. *Nature* **2001**, *414*, 345. (b) Schuster, M. F. H.; Meyer, W. H. *Annu. Rev. Mater. Res.* **2003**, *33*, 233.
- (3) Wainright, J. S.; Wang, J. T.; Weng, D.; Savinell, R. F.; Litt, M. J. *Electrochem. Soc.* **1995**, *142*, L121.
- (4) Kreuer, K. D.; Fuchs, A.; Ise, M.; Spaeth, M.; Maier, J. *Electrochim. Acta* **1998**, *43*, 1281.
- (5) Chen, W. F.; Wu, J. S.; Kuo, P. L. *Chem. Mater.* **2008**, *20*, 5756.
- (6) Casciola, M.; Chieli, S.; Costantino, U.; Peraio, A. *Solid State Ionics* **1991**, *46*, 53.
- (7) (a) Ponomareva, V. G.; Uvarov, N. F.; Lavrova, G. V.; Hairtudinov, E. F. *Solid State Ionics* **1996**, *90*, 161. (b) Otomo, J.; Minagawa, N.; Wen, C.-j.; Eguchi, K.; Takahashi, H. *Solid State Ionics* **2003**, *156*, 357. (c) Ponomareva, V. G.; Shutova, E. S. *Solid State Ionics* **2007**, *178*, 729.
- (8) (a) Bureekaew, S.; Horike, S.; Higuchi, M.; Mizuno, M.; Kawamura, T.; Tanaka, D.; Yanai, N.; Kitagawa, S. *Nat. Mater.* **2009**, *8*, 831. (b) Hurd, J. A.; Vaidhyanathan, R.; Thangadurai, V.; Ratcliffe, C. I.; Moudrakovski, I. L.; Shimizu, G. K. *Nat. Chem.* **2009**, *1*, 705. (c) Umeyama, D.; Horike, S.; Inukai, M.; Hijikata, Y.; Kitagawa, S. *Angew. Chem., Int. Ed.* **2011**, *50*, 11706.
- (9) (a) Hara, M.; Yoshida, T.; Takagaki, A.; Takata, T.; Kondo, J. N.; Hayashi, S.; Domen, K. *Angew. Chem., Int. Ed.* **2004**, *43*, 2955. (b) Tezuka, T.; Tadanaga, K.; Hayashi, A.; Tatsumisago, M. *J. Am. Chem. Soc.* **2006**, *128*, 16470. (c) Athens, G. L.; Ein-Eli, Y.; Chmelka, B. F. *Adv. Mater.* **2007**, *19*, 2580. (d) Lin, B.; Cheng, S.; Qiu, L.; Yan, F.; Shang, S.; Lu, J. *Chem. Mater.* **2010**, *22*, 1807. (f) Dey, C.; Kundu, T.; Banerjee, R. *Chem. Commun.* **2012**, *48*, 266. (e) Ponomareva, V. G.; Kovalenko, K. A.; Chupakhin, A. P.; Shutova, E. S.; Fedin, V. P. *Solid State Ionics* **2012**, DOI: 10.1016/j.ssi.2012.01.044.
- (10) Laberty-Robert, C.; Valle, K.; Pereira, F.; Sanchez, C. *Chem. Soc. Rev.* **2011**, *40*, 961.
- (11) Haile, S. M.; Boysen, D. A.; Chisholm, C. R. I.; Merle, R. B. *Nature* **2001**, *410*, 910.
- (12) Hoel, D.; Grunwald, E. *J. Phys. Chem.* **1977**, *81*, 2135.
- (13) Steininger, H.; Schuster, M.; Kreuer, K. D.; Kaltbeitzel, A.; Bingol, B.; Meyer, W. H.; Schauff, S.; Brunklaus, G.; Maier, J.; Spiess, H. W. *Phys. Chem. Chem. Phys.* **2007**, *9*, 1764.
- (14) Alberti, G.; Casciola, M. *Solid State Ionics* **2001**, *145*, 3.
- (15) (a) Kitagawa, S.; Kitaura, R.; Noro, S. *Angew. Chem., Int. Ed.* **2004**, *43*, 2334. (b) Banerjee, R.; Phan, A.; Wang, B.; Knobler, C.; Furukawa, H.; O'Keeffe, M.; Yaghi, O. M. *Science* **2008**, *319*, 939.
- (c) Férey, G. *Chem. Soc. Rev.* **2008**, *37*, 191. (d) Shimizu, G. K. H.; Vaidhyanathan, R.; Taylor, J. M. *Chem. Soc. Rev.* **2009**, *38*, 1430. (e) Zacher, D.; Shekha, O.; Woll, C.; Fischer, R. A. *Chem. Soc. Rev.* **2009**, *38*, 1418. (f) Farha, O. K.; Hupp, J. T. *Acc. Chem. Res.* **2010**, *43*, 1166. (g) Ohkoshi, S.; Nakagawa, K.; Tomono, K.; Imoto, K.; Tsunobuchi, Y.; Tokoro, H. *J. Am. Chem. Soc.* **2010**, *132*, 6620. (h) Shigematsu, A.; Yamada, T.; Kitagawa, H. *J. Am. Chem. Soc.* **2011**, *133*, 2034. (i) Wiers, B. M.; Foo, M.-L.; Balsara, N. P.; Long, J. R. *J. Am. Chem. Soc.* **2011**, *133*, 14522.
- (16) Paddison, S. J.; Kreuer, K. D.; Maier, J. *Phys. Chem. Chem. Phys.* **2006**, *8*, 4530.
- (17) Hayashi, S.; Hayamizu, K. *Bull. Chem. Soc. Jpn.* **1989**, *62*, 3061.
- (18) (a) Reinert, P.; Logar, N. Z.; Patarin, J.; Kaucic, V. *Eur. J. Solid State Inorg. Chem.* **1998**, *35*, 373. (b) Akamatsu, T.; Kasuga, T.; Nogami, M. *Adv. Mater. Res.* **2007**, *15–17*, 327.
- (19) (a) Yamada, M.; Honma, I. *Angew. Chem., Int. Ed.* **2004**, *43*, 3688. (b) Nakayama, M.; Sugiura, Y.; Hayakawa, T.; Nogami, M. *Phys. Chem. Chem. Phys.* **2011**, *13*, 9439.
- (20) (a) Hodge, I. M.; Ingram, M. D.; West, A. R. *J. Electroanal. Chem. Interfacial Electrochem.* **1975**, *58*, 429. (b) Hodge, I. M.; Ingram, M. D.; West, A. R. *J. Electroanal. Chem. Interfacial Electrochem.* **1976**, *74*, 125.
- (21) (a) Bauerle, J. E. *J. Phys. Chem. Solids* **1969**, *30*, 2657. (b) Hooper, A. J. *Phys. D: Appl. Phys.* **1977**, *10*, 1487.
- (22) Barsoukov, E.; Macdonald, J. R. *Impedance Spectroscopy*; Wiley-Interscience: New York, 2005.
- (23) Kreuer, K. D. *Chem. Mater.* **1996**, *8*, 610.
- (24) Alberti, G.; Casciola, M.; Costantino, U.; Vivani, R. *Adv. Mater.* **1996**, *8*, 291.
- (25) (a) Troup, J. M.; Clearfield, A. *Inorg. Chem.* **1977**, *16*, 3311. (b) Alberti, G.; Casciola, M.; Costantino, U.; Leonardi, M. *Solid State Ionics* **1984**, *14*, 289. (c) Ogawa, T.; Ushiyama, H.; Lee, J.-M.; Yamaguchi, T.; Yamashita, K. *J. Phys. Chem. C* **2011**, *115*, 5599.
- (26) Lee, Y. J.; Murakhtina, T.; Sebastiani, D.; Spiess, H. W. *J. Am. Chem. Soc.* **2007**, *129*, 12406.
- (27) (a) Bassat, J. M.; Odier, P.; Villesuzanne, A.; Marin, C.; Pouchard, M. *Solid State Ionics* **2004**, *167*, 341. (b) Yoshio, M.; Mukai, T.; Ohno, H.; Kato, T. *J. Am. Chem. Soc.* **2004**, *126*, 994. (c) Yoon, M.; Suh, K.; Kim, H.; Kim, Y.; Selvapalam, N.; Kim, K. *Angew. Chem., Int. Ed.* **2011**, *50*, 7870.
- (28) Gerhardt, R. *J. Phys. Chem. Solids* **1994**, *55*, 1491.
- (29) Vilčiauskas, L.; Tuckerman, M. E.; Bester, G.; Paddison, S. J.; Kreuer, K. D. *Nat. Chem.* **2012**, *4*, 461.